

Non-Linear Fluid-Coupled Computational Model of the Mitral Valve

Daniel R. Einstein¹, Karyn S. Kunzelman², Per G. Reinhall³, Mark A. Nicosia⁴,
Richard P. Cochran²

Departments of ¹Bioengineering and ³Mechanical Engineering, University of Washington, Seattle, Washington, ²Central Maine Heart and Vascular Institute, Central Maine Medical Center, Lewiston, Maine, ⁴Department of Biomedical Engineering, University of Minnesota, Minneapolis, Minnesota, USA

Background and aim of the study: The dynamics of the mitral valve result from the synergy of left heart geometry, local blood flow and tissue integrity. Herein is presented the first coupled fluid-structure computational model of the mitral valve in which valvular kinematics result from the interaction of local blood flow and a continuum representation of valvular microstructure.

Methods: The diastolic geometry of the mitral valve was assembled from previously published experimental data. Anterior and posterior leaflets were modeled as networks of entangled collagen fibers, embedded in an isotropic matrix. The resulting non-linear continuum description of mitral tissue was implemented in a three-dimensional membrane formulation. Chordal tension-only behavior was defined from experimental tensile tests. The computational model considered the valve immersed in a domain of Newtonian blood, with an experimentally determined viscosity corresponding to a shear rate of

180 s^{-1} at 37°C . Ventricular and atrial pressure curves were applied to ventricular and atrial surfaces of the blood domain.

Results: Peak closing flow and volume were 51 ml/s and 1.17 ml, respectively. Papillary muscle force ranged dynamically between 0.0 and 2.6 N. Acoustic pressure (RMS) was found to be 3.3 Pa, with a peak frequency of 72 Hz at 0.064 s from the onset of systole. Model predictions showed excellent agreement with available transmitral flow, papillary force and first heart sound (S1) acoustic data.

Conclusion: The addition of blood flow and an experimentally driven microstructural description of mitral tissue represent a significant advance in computational studies of the mitral valve. This model will be the foundation for future computational studies on the effect of pathophysiological tissue alterations on mitral valve competence.

The Journal of Heart Valve Disease 2005;14:376-385

The mitral valve allows unidirectional flow from the atrium to the ventricle by resisting the pressure of the left ventricle during systolic contraction. The term 'mitral apparatus' encompasses the mitral annulus, anterior and posterior leaflets, chordae tendineae and papillary muscles. The annulus marks the border between the left atrium and the left ventricle; the chordae, attached to the surface of the leaflets, reach out to the papillary muscles located on the inner left ventricular wall. From a macro-mechanical point of view, it is the synergistic function of these structures - the passive closure under flow of the mitral leaflets, and the

active contraction of the papillary muscles and mitral annulus - that assure controlled coaptation of the two leaflets. From a micro-mechanical point of view it is the integrated properties of the tissue constituents - primarily collagen and elastin - that determine the functional (or dysfunctional) response of the parts.

The arrangement of collagen and elastin in normal mitral leaflets and chordae is both complex and purposeful. For example, there are varying amounts of collagen throughout the mitral apparatus, and both local collagen splay and orientation are highly heterogeneous (1-3). It is well known that the mechanical behavior of collagen fibers is highly non-linear (4). However, the local spatial distribution of collagen fibers confers mitral tissue with a high degree of anisotropy and non-linear coupling not seen in single collagen fibers (4,5). A generally accepted paradigm for mitral tissue mechanics in terms of its components views this non-linearity and anisotropy as resulting from both the progressive straightening and alignment

Address for correspondence:

Karyn S. Kunzelman PhD, Central Maine Medical Center and Central Maine Heart and Vascular Institute, 10 High Street, Suite 305, Lewiston, ME 04240, USA
Tel: 207-753-3910
Fax: 207-753-3903
e-mail: Kkunzelman@cmhc.org

of collagen fibers in the direction of load.

The aim of the present study was to develop a coupled fluid-structure simulation of mitral valve closure in which the mitral leaflet behavior results from a continuum representation of this structural paradigm. Model predictions for closing flow, regurgitant volume, dynamic papillary muscle force and non-stationary acoustic radiation were compared to published data in order to assess the predictive capability of the model, and to establish a foundation for future studies examining the relationship between mitral tissue integrity and mitral valve function and dysfunction.

Materials and methods

Finite element method

The commercial finite element program, LS-DYNA (Livermore Software Technology Corporation, Livermore, CA, USA), was used to perform all simulations. LS-DYNA is a transient hydrocode, typically applied to high-speed compressible flows. The applicability of this to low-speed viscous flows characteristic of the cardiac environment has recently been demonstrated (6). Custom subroutines to describe the non-linear anisotropic behavior of mitral tissue were added, and have been described previously (6).

Model geometry

The mid-diastolic surface geometry of the mitral valve leaflets and papillary muscle tips, as well as the number and radiation pattern of the chordae tendineae, were developed from fresh porcine hearts (7). It has been found that porcine mitral valve is the closest non-human analog in terms of leaflet surface geometry, chordal number and arrangement, and overall valvular proportions (8,9). The techniques used to distil the physical geometry of the porcine hearts into coordinates for input to the finite element model have been described previously (7,9). Consistent with anatomical studies, 12 chordae radiate from three heads representing the anterior papillary tip (7). Five times as many chordae attach to the margin and belly of each leaflet (7). Thickness data for the leaflets were also derived from published anatomical studies (7).

Dynamic video fluoroscopic data have suggested that the mitral annulus is approximately symmetric about the septal-lateral midline (10-13). However, significant asymmetry exists with regard to subvalvular geometry and motion, both in normal function and in pathology (11-14). Nevertheless, to limit the computational overhead associated with modeling both the mitral valve and its fluid medium, the choice was made to construct a model from the septal-lateral midline to the anterior wall, and to apply symmetry boundary conditions on the septal-lateral mid-plane.

In addition, the ventricular or atrial geometries were not modeled. Instead, the valve was immersed in a regular fluid domain appropriate for eventual in-vitro verification (Fig. 1). Atrial and ventricular pressure-load curves were applied to the atrial and ventricular surfaces of the fluid domain. Both curves were based on porcine in-vivo measurements made in the authors' laboratory with a Millar MIKRO-TIP catheter (Millar Instruments, Inc., Houston, TX, USA). Pressure crossover occurred at 0.032 s from the beginning of simulation. Only the closing phase of the mitral valve was modeled. This represented a 150 ms time frame between the beginning of the simulation and the cessation of flow.

Material and elemental assumptions

Leaflets

As the bending behavior of mitral leaflet tissue has never been quantified, it was assumed that the leaflets acted as membranes. In other words, it was assumed that bending produces insignificant moments. The FORTRAN code for this membrane formulation has been fully described (6). Mean collagen fiber angles were mapped to both anterior and posterior leaflets from previously acquired small-angle light-scattering data (14). The anterior and posterior leaflets were discretized into 740 elements each. The commissure was modeled with 180 elements. Both leaflets and the commissure were coupled to the fluid.

Mitral leaflet tissue material behavior was character-

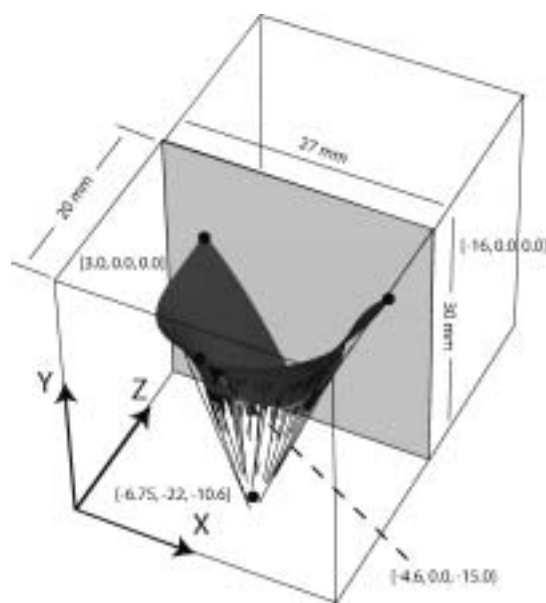


Figure 1: Symmetry conditions and dimensions of fluid domain. The coordinates of three points: 1) the papillary muscle tip; and 2, 3) the symmetry points of the anterior and posterior annuli are given with respect to the indicated coordinate system for reference.

Table I: Leaflet material parameters.

Location	A (kPa)	B	σ	α (kPa)	κ (kPa)	ρ (kg/mm ³)
Anterior	0.070	40	19.9°	10	2.5×10 ⁴	1.04×10 ⁻⁶
Posterior	0.005	40	19.9°	10	2.5×10 ⁴	1.04×10 ⁻⁶
Commissure	0.030	40	19.9°	10	2.5×10 ⁴	1.04×10 ⁻⁶

ized as an oriented Gaussian distributed population of crimped collagen fibers embedded in an isotropic phase of gel-like glycoproteins and a network of isotropic elastin (Fig. 2). Mathematically, the stress-strain behavior (Fig. 3) of the mitral leaflets was characterized by the structural constitutive equation (15):

$$\mathbf{S} = p\mathbf{J}\mathbf{C}^{-1} + 2\mathbf{J}^{-2/3}\text{DEV}\left[\frac{\partial\tilde{W}}{\partial\tilde{\mathbf{C}}}\right]$$

$$\frac{\partial\tilde{W}}{\partial\tilde{\mathbf{C}}} = \alpha\mathbf{I} + \int_{-\pi/2}^{\pi/2} S_f \mathbf{R}(\theta)\mathbf{A} \otimes \mathbf{A} d\theta$$

$$S_f = A \left[\exp\left[\frac{B}{2}(\mathbf{A}(\theta)\mathbf{C}\mathbf{A}(\theta) - 1)\right] - 1 \right]$$

$$\mathbf{R}(\theta) = \frac{1}{\sigma\sqrt{2\pi}} \exp\left[\frac{-(\theta - \mu)^2}{2\sigma^2}\right]$$
(1)

where \mathbf{S} is the second Piola-Kirchhoff stress, p the hydrostatic pressure, \mathbf{J} the Jacobian, S_f the collagen stress-strain behavior, \mathbf{I} the identity matrix, \mathbf{A} the orientation tensor, σ a statistical parameter related to fiber splay, μ the mean fiber direction and A and B are material parameters. The above relationship is described in greater detail by Einstein et al. (6).

The material parameters A , B and σ were derived

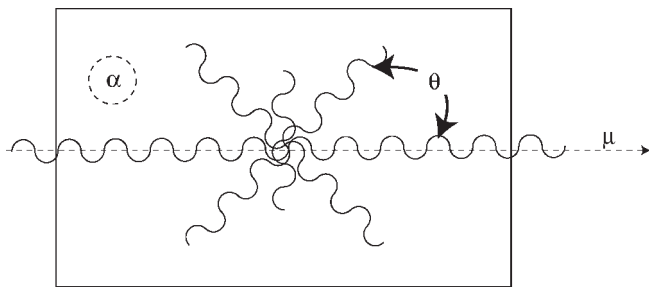


Figure 2: Structural paradigm for mitral leaflet tissue. Collagen fibers (wavy lines) are embedded in an isotropic matrix (α). Locally, the fibers have a mean preferred direction (μ). The standard deviation (σ) determines the Gaussian distribution of collagen fibers about that mean as a function of the splay angle (θ).

from fitting Eq. (1) to published biaxial data for mitral valve anterior and posterior leaflet (16). Material parameters for both anterior and posterior leaflet are listed in Table I.

Chordae

The chordae were modeled as tension-only cables. Although it is widely believed that the chordae act as secondary orifices for blood flow, the chordae were not coupled to the fluid. Chordal diameters are listed in Table II.

The stress-strain behavior of the chordae tendineae, like that of the mitral leaflet tissue, was non-linear. As the chordae are uniaxial, experimental data may be directly input for chordae material behavior. Chordal stress-strain data were digitized from published data (17).

Blood

An Eulerian formulation was used to model the blood domain. Blood was modeled as a compressible, Newtonian fluid. Specifically, the deviatoric stress depended linearly on the shear rate, while compressibility was governed by the equation of state:

$$P - P_o = K(J - 1)$$
(2)

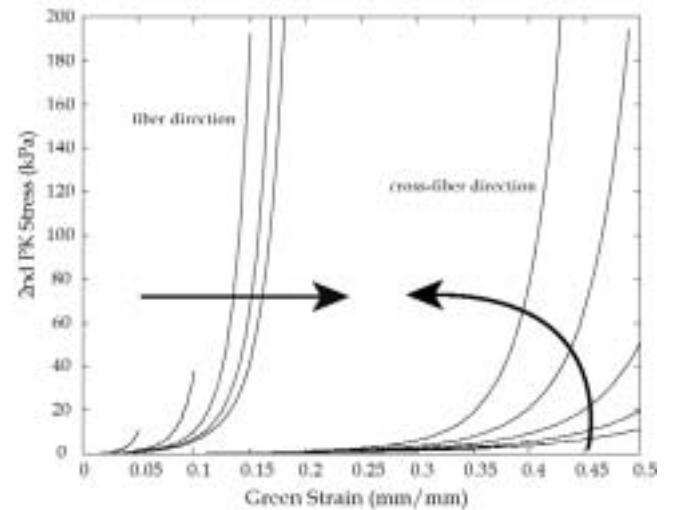


Figure 3: Anterior mitral valve, fiber and cross-fiber directions. Arrows indicate the effect of increasing strain levels in the orthogonal direction.

Table II: Chordal geometric properties.

Chord	ρ (kg/mm ³)	Cross-section (mm ²)
Strut chord	1.04×10^{-6}	1.15
Primary basal	1.04×10^{-6}	0.79
Sub-basal	1.04×10^{-6}	0.23
Primary marginal	1.04×10^{-6}	0.45
Sub-marginal	1.04×10^{-6}	0.15

where P is the pressure, K the blood bulk modulus, and J the Jacobian or volume ratio.

For computational efficiency, without sacrificing accuracy (6), the bulk modulus was lowered to 2.5×10^4 kPa from 2.5×10^6 kPa. Blood viscosity was determined from published data collected in a cone-in-plate viscometer at 37°C and a shear rate of 180 s^{-1} (18). An average non-anemic value of 0.045 poise (kg/mm·s) was adopted. Density was set to 1.00×10^{-6} kg/mm³. The dimensions of the fluid domain were 20×30×20 mm. To investigate grid sensitivity, the fluid domain was modeled with 35×53×48 fluid elements and with 70×100×90 elements.

To determine the acoustic pressure, the pressure of six central fluid elements was sampled at 2.5 kHz and zero padded to $n = 1,024$. The averaged signal was bandpass filtered from 40 to 1,000 Hz with a 5th-order Butterworth filter (see Fig. 10). The root mean-squared (RMS) value was computed as:

$$S1_{\text{RMS}} = \frac{1}{N} \left[\sum_{n=1}^N S1_n^2 \right]^{1/2} \quad (3)$$

on the original unpadding signal.

Measured S1

In order to determine a benchmark for the frequency response of simulated S1, thoracic phonocardiographic measurements of anesthetized juvenile farm sheep

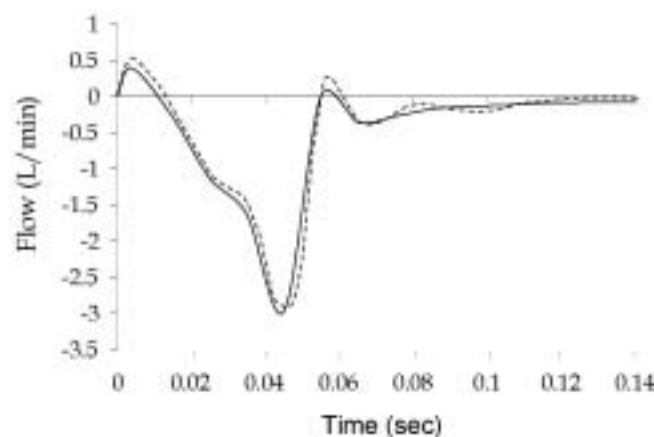


Figure 4: Mitral valve closing flow. Black line: coarse fluid grid (35?53?48). Red line: fine fluid grid (70?100?90).

($n = 9$) were performed. Measurements were made with a hydrogel-applied surface wave transducer (FlowScan, Lisa-150 auscultation system), with a 5th-order Butterworth bandpass filter of 50 to 1,000 Hz. The conditioned and amplified signal was recorded in digital format at a rate of 2,500 Hz, and subsequently low-passed to 1,000 Hz. A simultaneous electrocardiographic waveform (ECG) was recorded for off-line segmentation of the heart sounds into the first heart sound (S1) and the second heart sound (S2). A custom algorithm for segmenting the sounds, parsed S1 into blocks of 512 samples from the QRS wave, corresponding to the onset of systole. At most, eight successive beats were collected preoperatively and postoperatively for each animal.

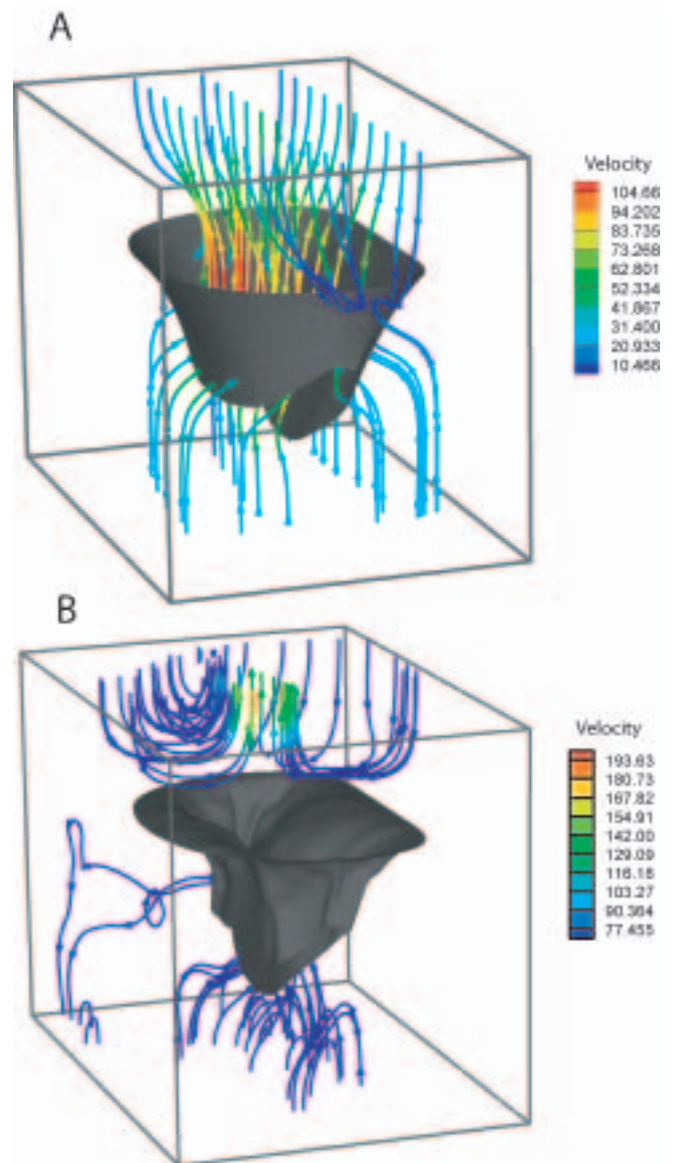


Figure 5: Streamtraces of blood velocity in the initial ($t = 20 \text{ ms}$) and final ($t = 85 \text{ ms}$) phases of closure. Note: The velocity ranges differ from A to B for clarity.

Results

Flow

In keeping with convention, transmitral flow was defined in such a way that negative flow was towards the atrium, and positive flow was towards the ventricle. Peak closing flow was computed as 51 ml/s (Fig. 4). Regurgitant closing volume, the time-integral of transmitral closing flow, was 1.17 ml per beat. Peak backward velocity into the atrium was 887 mm/s (Fig. 6A). Transmitral flow was also determined at the higher grid density to examine discretization errors. Flow at the higher grid density was found to not significantly differ from that at the lower grid density.

Figure 5A shows fluid flow through the mitral valve during the initial phase of closure ($t = 0.02$ s), while

Figure 5B shows fluid flow in the final phase of closure ($t = 0.085$ s). Where streamtraces appeared to penetrate the leaflets, the leaflets were moving with the local fluid velocity. The chordae are not shown for the sake of clarity. The sequence shown in Figure 6A-B, illustrates the development of flow during closure. Though the flow was fully three-dimensional (Fig. 5A,B) the streamtraces in Figure 6A and B were plotted on the plane of symmetry to confine them to a two-dimensional plane for more facile interpretation. The eddy structures in Figure 6B above the mitral valve should be noted.

Papillary muscle force

Papillary muscle force was determined as the sum of the reaction forces on the three nodes that represented the three heads of the anterolateral papillary muscle. The time course of papillary muscle force closely followed the left ventricular pressure curve (Fig. 7B), with a maximum of 2.6 N at a transvalvular pressure (LV-LA) of 95 mmHg. A notch in the papillary force curve at about 0.06 s from the beginning of simulation

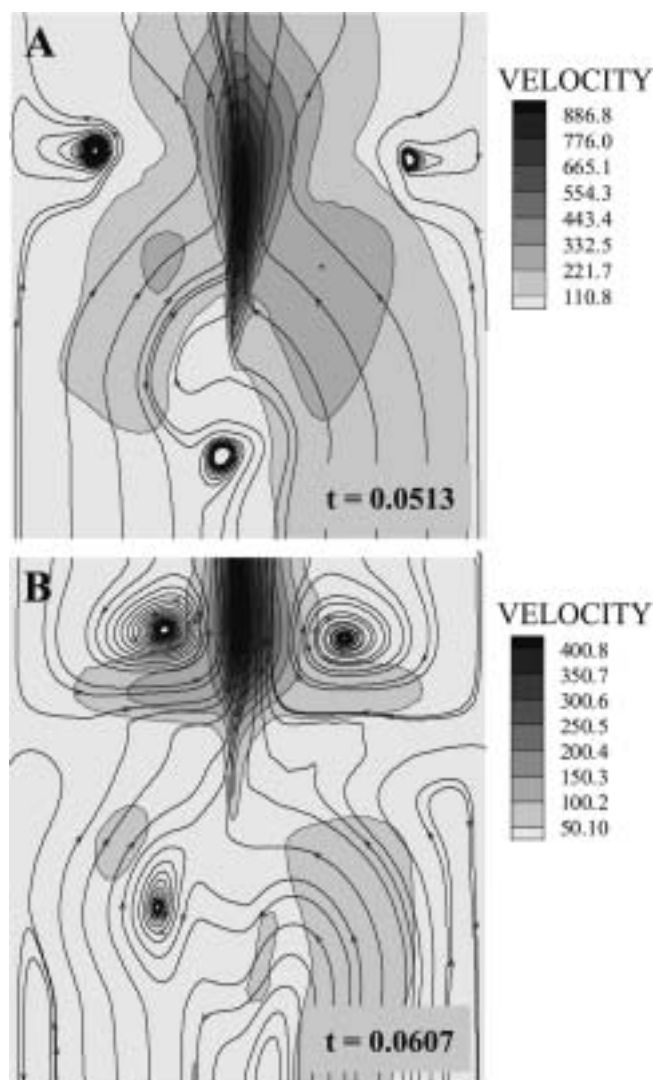


Figure 6: Flow velocity projected onto the septal-lateral plane. Note: For visual clarity the contour levels differ for each plane.

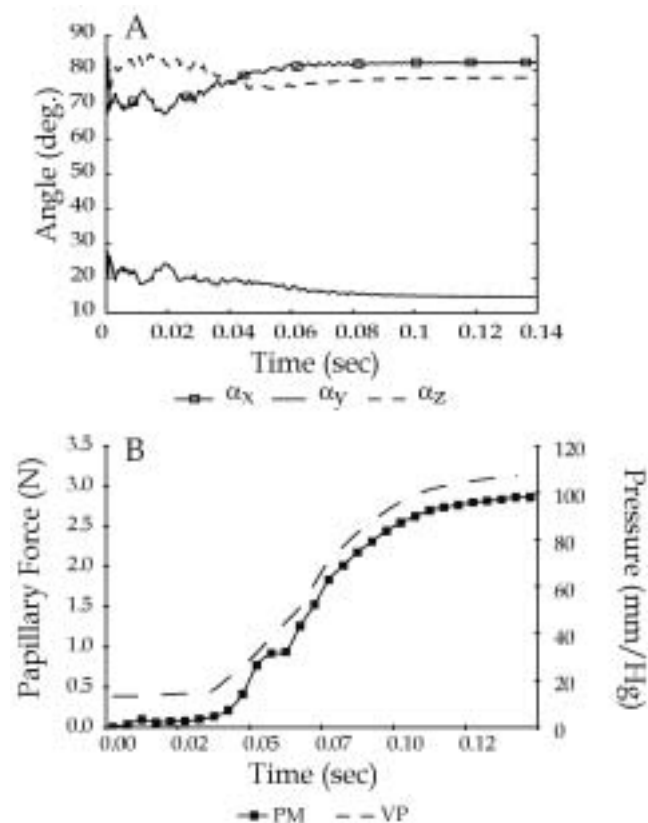


Figure 7: Anterolateral papillary muscle force. A: Direction cosines of papillary muscle force with respect to coordinate system in Figure 1. B: Ventricular pressure and total papillary force magnitude. The broken line indicates ventricular pressure; open squares indicate papillary force.

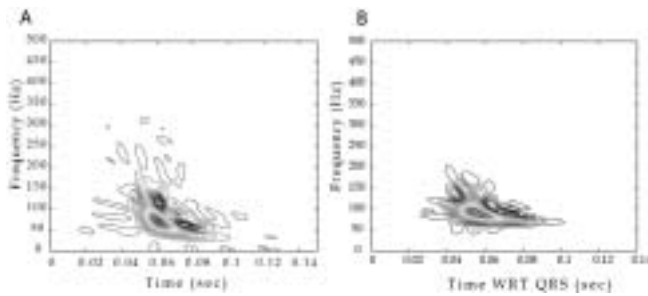


Figure 8: Simulated intraventricular S1 (A) and measured thoracic S1 (B).

corresponded to the onset of coaptation and valvular vibration. Maximum tension in the strut chord - the largest basal chord inserted to the anterior leaflet - was found to be 0.52 N. The direction of the papillary muscle force varied slightly from beginning to end of the simulation (Fig. 7A).

Frequency response of S1 Computational model

The sampled and filtered average pressure signal from the computational model was analyzed in the time-frequency plane with a Wigner-Ville distribution and a radially Gaussian kernel. The transformed signal (Fig. 8A), was found to have a downward glide in fre-

quency with a maximum at 72.0 Hz occurring at 0.0604 s from pressure crossover. The RMS of the acoustic pressure was 3.3 Pa.

Animal model

The collected and segmented signals were analyzed analogously to the simulated pressure signal. The thoracic S1 were found to have a flat or semi-lunar shape. A typical thoracic S1 is shown in Figure 8B. The average maximum peak frequency was 71.7 ± 2.8 Hz, and occurred at 0.071 ± 0.003 s from the peak of the QRS wave in the ECG.

Stress and strain

Late diastolic and early systolic peak principal stress occurred in the trigone of the anterior leaflet (Fig. 9A). By 0.047 s, at a transvalvular pressure of about 11.8 mmHg, the valve was mostly closed and the peak principal stress drained from the strut chorda to the trigones. This was slightly before the peak frequency component in the acoustic pressure at 0.06 s (Fig. 8A). At 0.07 s the valve was fully closed and oscillating. The peak stress was 140 kPa, and was in the belly of the leaflet and at the insertion of the strut chorda. This corresponded to a transvalvular pressure of 48.0 mmHg. By 0.093 s and a transvalvular pressure of 75.4 mmHg, the stress had risen to 224 kPa and the stress pattern was stable. At the final transvalvular pressure of 98 mmHg at 0.14 s, the stress had leveled off to 254 kPa.

Circumferential strains (Almansi) were highly negative on both leaflets towards the commissures, and particularly in the neighborhood of the physiological wrinkles (Fig. 10A), ranging from 0.17 to -0.51. Radial strains, however, were entirely tensile, ranging from 0.04 to 0.25 (Fig. 10B).

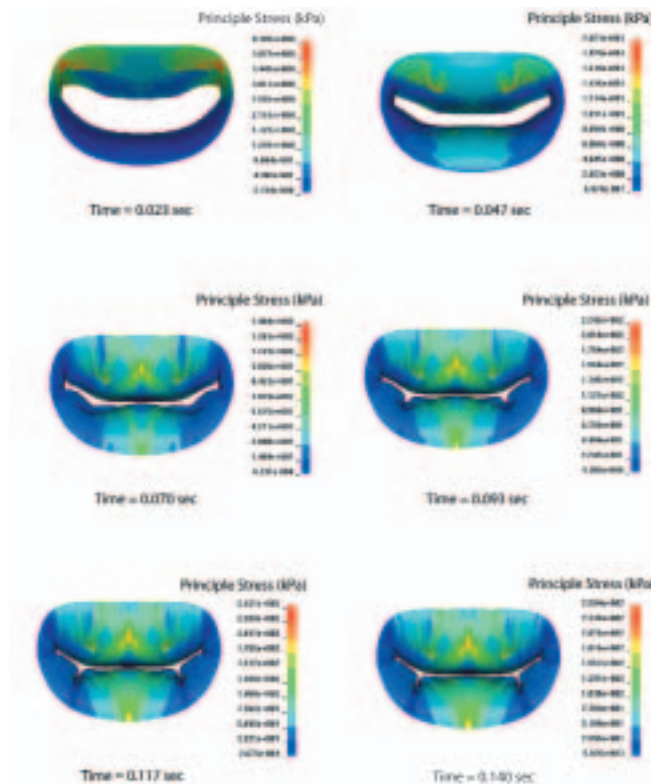


Figure 9: Time course of principal stress. Note: For visual clarity, the contour levels differ for each plane.

Discussion

The results have been described of a three-dimensional coupled fluid-structure computational model of the mitral valve that incorporates a continuum representation of mitral leaflet microstructure. The aim of the present investigation was to study the effect of pathophysiological tissue alterations on mitral valve competence and mitral valve acoustic radiation. The

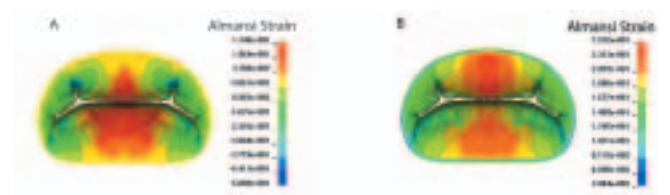


Figure 10: Circumferential (A) and radial (B) Almansi strain at 0.14 s.

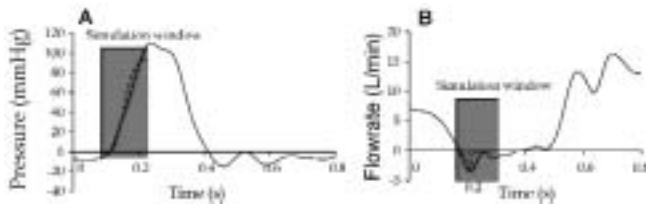


Figure 11: Transvalvular pressure (A) and transmitral flow (B). The black line indicates data from reference [23]; the red line indicates data from the computational model. Input transvalvular pressure was shifted to match the early systolic zero-crossing in the measured transvalvular pressure. The predicted closing flow (red line) shows excellent agreement with in-vitro data (black line) over the simulation window. Note: The predicted flow data was shifted an additional 50 ms to the right due to the inertia-driven lag between pressure and flow in the measured data. (Measured data reprinted from Jensen KT, Fontaine A, Yoganathan AP. Improved in vitro quantification of the force exerted by the papillary muscle on the left ventricular wall: three-dimensional force vector measurement system. *Ann Biomed Eng* 2001;29:406-413; ©2001, with permission from AMBE.)

longer-term goals of the present study are to use advanced computer methods to guide non-invasive diagnostic development and to guide surgical intervention. Herein, attention was focused on the closing phase of mitral dynamics in order to lay the foundation for future computational studies on the effect of pathophysiological tissue changes on mitral valve competence. In the following section, the structural and fluid dynamic behavior of the model is discussed, and model predictions compared to available data.

Flow

Blood flow was modeled as laminar - that is, turbulent energy losses at a scale below the level of the mesh were neglected. It is unclear whether turbulence develops during normal function. However, turbulence that accompanies mitral regurgitation has been amply documented. The choice was made to begin with a fully unsteady laminar flow and its interaction with the valve leaflets, with the understanding that large-scale eddy structures would be the most important with respect to the global coupled behavior of the blood immersed valve.

Flow was determined for both coarse and fine fluid grid densities. Doubling the grid density of the fluid domain did not substantially alter the predicted transmitral flow (Fig. 4), suggesting that the lower grid density was sufficient to capture the physics of the interaction.

The complex atrial and ventricular flow fields make the in-vivo quantification of transmitral flow difficult,

and only semi-quantitative. Nevertheless, the profile of the predicted mitral closing flow (Fig. 4) was similar to those determined using M-mode echocardiography (19,20). The closing volume for normal dogs, measured using M-mode echocardiography, has been reported as 3.23 ml per heart beat (20). This value agreed well with a predicted closing volume of 1.17 ml. It should be noted that specific closing volumes would be a function of the size of the annular orifice, as well as hemodynamic indicators such as heart rate.

Furthermore, the peak closing flow for mechanical prosthetic valves in the mitral position has been reported to be on the order of 120 ml/s, with closing volumes ranging between 4 and 6% of that value (21). Thus, both the modeled peak flow and closing volume were considerably lower than peak flows and closing volumes for mechanical valves, as would be expected.

Predicted transmitral flow also showed excellent agreement with published in-vitro transmitral flow data obtained with the Georgia Tech left heart simulator (22). Specifically, the peak closing flow of 3.1 l/min compared well with a measured peak closing flow of 3.6 l/min (Fig. 11B). No attempt was made to normalize for potentially different anatomical or material properties, or for different inputs (Fig. 11A). In addition, the difference in initial conditions produced a temporal lag of about 50 ms between the backward measured flow and the backward simulated flow. This temporal lag between pressure crossover and closure was also seen in vivo, where inertia of the filling flow continued to pour into the ventricle slightly after equilibrium was reached (23). Because diastole was not modeled, there was no lag between pressure crossover and retrograde leaflet motion.

The role that filling vortices play in pushing against the leaflets to bring them together is disputed (23). Again, because diastole was not modeled, forward flow did not produce visible eddies behind the leaflets. However, backward flow produced vortices above the valve immediately after coaptation (Fig. 6). To the present authors' knowledge, these vortex structures have not been previously reported. It is possible that the geometry and compliance of the atrium may influence or even dissipate these structures. This point warrants further study as it may affect the accuracy of clinical estimations of regurgitant volume and velocity.

Papillary muscle force

The relationship between papillary muscle force and the left ventricular pressure curve is well documented (22,24,25). Specific peak values for papillary muscle force show some variability. Clearly, values will depend on the magnitude of transvalvular pressure and, at least transiently, on the pressure derivative. For example, Hashim et al. found the papillary muscle

force in an in-vitro set-up to follow the left ventricular pressure curve, with no early systolic notch and a value of 2.5 N, corresponding to a maximum transvalvular pressure of about 80 mmHg (24). In later in-vitro measurements made by Jensen et al., the papillary muscle force was about 2.5 N at 80 mmHg, and varied almost linearly with increased end-systolic pressure (22). The predicted value of 2.6 N agreed quite well with either of these measurements.

Chordal tension

The papillary force was found to be distributed unevenly among the basal chords - that is, those that insert toward the annulus on both leaflets - with the chords of the anterior leaflet bearing the greatest load. This was in agreement with previous models (9,26). The strut chord (the thickest of the anterior basal chords) is generally assumed to carry the largest load, and this assumption was confirmed in the present model. Maximum tension in the strut chord was found to be 0.52 N. An in-vivo measurement of strut chord tension in dogs identified a value of about 0.60 N at 100 mmHg (10). Although this measurement is difficult because of its obviously intrusive nature, the simulated and measured values were generally in agreement.

Acoustic response

It is now widely recognized that S1 is non-stationary - that is, its frequency components change with respect to time. This non-stationarity was observed in both the computational model and the measured thoracic S1. The predicted time-frequency signature was found to have a downward glide in frequency, with a maximum at 72.0 Hz occurring at 0.0604 s from pressure crossover. Similarly, the average maximum peak frequency for the measured thoracic sounds was 71.7 ± 2.8 Hz, and occurred 0.071 ± 0.003 s from the peak of the QRS wave in the ECG. Chen et al. also found that measured intraventricular S1 were either flat or in the shape of a descending crescent in the time-frequency plane (27-29), suggesting a qualitative agreement between measured intraventricular S1 and the predicted 'intraventricular' S1. In addition, the predicted RMS acoustic pressure was of the same order of magnitude as RMS values of measured intraventricular S1 (30). Correlations were not made between measured thoracic and simulated 'intraventricular' amplitude, as it is well known that thoracic S1 are filtered and attenuated versions of the intraventricular S1 (31-34). It must be noted that for S1 to be useful in a clinical setting does not necessarily require the thoracic and intraventricular sounds to be quantitatively similar, only that the transmitted character be preserved.

In order to focus on the mitral valve alone, shape,

impedance and motion of the ventricle and atrium were not modeled. The excellent agreement between predicted and measured values - despite these simplifications - lends a strong argument to the valvular origin of S1 and lays the groundwork for future companion studies that relate tissue microstructure to S1 acoustic patterns in disease.

Stress and strain

The peak principal stress of 254 kPa was 30% lower than the maximum principal stress predicted by earlier models (9). Interestingly, both radial and circumferential stresses were tensile for both of the leaflets throughout the simulation, while circumferential Almansi strains were highly compressive on both leaflets toward the commissures, and particularly in the neighborhood of the physiological wrinkles (Fig. 10).

This diametric behavior of stress and strain has been noted previously in in-vitro biaxial tests of cardiac tissue (15,35), and is a fundamental difference between linear and non-linear behavior. It is believed that this coupled behavior is influenced by the fiber splay. In the present simulation, both mitral leaflets have been assigned uniform material properties. The challenge of determining the spatially local fiber splay and volume fraction remain outstanding biomechanical problems.

Study limitations

Any model necessarily embodies simplifications and limitations. In this first study, the focus was on the gross dynamics of the mitral valve immersed in fluid, and in particular on the resulting acoustic radiation. Mitral leaflets were discretized with single-point membrane elements. The membrane assumption necessarily implies some error in stress-strain behavior of the leaflets, as well as the near-field fluid-coupled behavior of the valve as a whole. In addition, assumptions were made with regard to the fluid behavior and, indeed, with regard to the model geometry.

As for the stress-strain behavior, there are fundamentally three important assumptions to consider. First, membrane elements embody a plane-stress assumption; in other words, the thickness direction stress is assumed to be negligibly small. During the normal cardiac cycle, peak transvalvular pressure is on the order of 16 kPa. This is, indeed, small compared to the predicted peak stress of 254 kPa, though perhaps not vanishingly small. Second, no bending effects were considered for the leaflets. At present, little is known quantitatively about mitral leaflet bending behavior. However, mitral bending stiffness is generally considered to be small with respect to in-plane stiffness. Finally, the material parameters were considered to be uniform across the valve leaflets. The considerable dif-

ference in mechanical behavior between the anterior and posterior leaflets suggests that, in addition to variation in principal fiber angles, there is also much regional variation of leaflet material behavior.

Adopting a membrane to represent a three-dimensional structure in a fluid, also implies a limitation in the representation of local fluid-flow in the neighborhood of the valve leaflets. The frames in Figures 5, 9 and 10 reveal a gap between the two leaflets, in spite of coaptation. This gap is a visual artifact, in the sense that the elements represent the leaflet mid-surface, and thus one leaflet is visually offset from the other, though both are in contact. Nevertheless, the flow-interaction on the leaflets edge does not account for this thickness.

The geometry of the model was derived from the averaging of several porcine valves, including chordal lengths and insertions (7,8). In addition, only half of the valve was modeled, and an assumption of symmetry was made. There is much valve-to-valve variation in chordal insertion and indeed, in general mitral anatomy. Chordal insertion, in particular, will have a profound effect on the dynamics of the model and on chordal kinetics. In addition, the fluid domain was modeled as a box, which facilitates comparison with published in-vitro data. However, the three-dimensional behavior of blood flow in vivo will be strongly dependent on atrioventricular geometry and kinematics.

In conclusion, despite the many assumptions that were included in this first non-linear fluid-coupled model, the predictions closely matched a wide range of available data. Thus, this coupled fluid-structure model constituted a valid tool for investigating the interaction between flow and mitral conformational abnormalities, and the functional boundaries between normal and diseased mitral tissue as a function of tissue microstructure. In addition, these studies form the foundation of a computational framework to aid in the refinement and development of non-invasive diagnostic evaluation.

References

1. Burge EC. A microstructural and biochemical analysis of the mitral valve. In: Bioengineering. University of Washington, Seattle, 1996:357
2. Cole WG, Chan D, Hickey AJ, Wilcken DE. Collagen composition of normal and myxomatous human mitral heart valves. *Biochem J* 1984;219:451-460
3. Kunzelman KS, Cochran RP, Murphree SS, Ring WS, Verrier ED, Eberhart RC. Differential collagen distribution in the mitral valve and its influence on biomechanical behavior. *J Heart Valve Dis* 1993;2:236-244
4. Fung Y.-C.B. Biomechanics: Mechanical properties of living tissues. Springer-Verlag, New York, 1993
5. Fung YC. Microrheology and constitutive equation of soft tissue. *Biorheology* 1988;25:261-270
6. Einstein DR. Nonlinear acoustic analysis of the mitral valve. In: Bioengineering. Seattle, University of Washington, 2002
7. Kunzelman KS. Engineering analysis of mitral valve structure and function. In: Biomedical Engineering. University of Texas Southwestern Medical Center, Dallas, 1991
8. Kunzelman KS, Cochran RP, Verrier ED, Eberhardt RC. Anatomic basis for mitral valve modeling. *J Heart Valve Dis* 1994;3:491-496
9. Kunzelman KS, Cochran RP, Chuong C, Ring WS, Verrier ED, Eberhart RD. Finite element analysis of the mitral valve. *J Heart Valve Dis* 1993;2:326-340
10. Salisbury PF, Cross CE, Rieben PA. Chorda tendinae tension. *Am J Physiol* 1962;205:385-392
11. Komeda M, Glasson JR, Bolger AF, et al. Three-dimensional dynamic geometry of the normal canine mitral annulus and papillary muscles. *Circulation* 1996;94(Suppl. 9):159-163
12. Dagum P, Timek TA, Green GR, et al. Coordinate-free analysis of mitral valve dynamics in normal and ischemic hearts. *Circulation* 2000;102(Suppl.III):62-69
13. Komeda M, Glasson JR, Bolger AF, Daughters GT, Ingels NB, Miller DC. Papillary muscle-left ventricular wall 'complex'. *J Thorac Cardiovasc Surg* 1997;113:292-301
14. Cochran RP, Kunzelman KS, Chuong CJ, Sacks MS, Eberhart RC. Nondestructive analysis of mitral valve collagen fiber orientation. *Am Soc Artif Intern Org Trans* 1991;37:M447-M448
15. Billiar KL, Sacks MS. Biaxial mechanical properties of the native and glutaraldehyde-treated aortic valve cusp: Part II - A structural constitutive model. *J Biomech Eng* 2000;122:327-335
16. May-Newman K, Yin FC. A constitutive law for mitral valve tissue. *J Biomech Eng* 1998;120:38-47
17. Kunzelman KS, Cochran RP. Mechanical properties of basal and marginal mitral valve chordae tendinae. *Am Soc Artif Intern Org Trans* 1990;36:M405-M408
18. Stein PD, Sabbah HN. Accentuation of the heart sounds in anemia. *Am J Physiol* 1978;235:H664-H669
19. Laniado S, Yellin EL, Miller H, Frater RWM. Temporal relation of the first heart sound to closure of the mitral valve. *Circulation* 1973;45:1006-1013
20. Laniado S. A study of the dynamic relations between mitral valve echogram and phasic mitral flow. *Circulation* 1975;51:104-113
21. Feng Z, Nakamura T, Fujimoto T, Umezo M. In

- vitro investigation of opening behavior and hydrodynamics of bileaflet valves in the mitral position. *Artif Org* 2002;26:32-39
22. Jensen KT, Fontaine A, Yoganathan AP. Improved in vitro quantification of the force exerted by the papillary muscle on the left ventricular wall: Three-dimensional force vector measurement system. *Ann Biomed Eng* 2001;29:406-413
 23. Reul H, Talukder N, Muller EW. Fluid mechanics of the natural mitral valve. *J Biomech* 1981;14:361-372
 24. Hashim SR, Fontaine A, Shengqui H, Levine RA, Yoganathan AJ. A three-component force vector cell for in vitro quantification of force exerted by the papillary muscle on the left ventricular wall. *J Biomech* 1997;30:1071-1075
 25. Nielsen RA, Nygaard H, Fontaine A. Chordal force distribution determines systolic mitral leaflet configuration and severity of functional mitral regurgitation. *J Am Coll Cardiol* 1999;33:843-853
 26. Kunzelman K, Reimink MS, Verrier ED, Cochran RP. Replacement of mitral valve posterior chordae tendineae with expanded polytetrafluoroethylene suture: A finite element study. *J Card Surg* 1996;11:136-145; discussion 146
 27. Chen D, Durand LG, Lee HC, Wieting DW. Time-frequency analysis of the first heart sound: Part 3: Application to dogs with varying cardiac contractility and to patients with mitral mechanical prosthetic heart valves. *Med Biol Eng Comput* 1997;35:455-461
 28. Chen D, Durand LG, Lee HC. Time-frequency analysis of the first heart sound. Part 1: Simulation and analysis. *Med Biol Eng Comput* 1997;35:306-310
 29. Chen D, Durand LG, Guo Z, Lee HC. Time-frequency analysis of the first heart sound. Part 2: An appropriate time-frequency representation technique. *Med Biol Eng Comput* 1997;35:311-317
 30. Genest J, Durand LG. Relationship of the left ventricular and apical first sounds to the left ventricular derivative. *Med Biol Eng Comput* 1985;23:95-98
 31. Durand LG, Genest J, Guardo R. Modeling the transfer function of the heart-thorax acoustic system in dogs. *IEEE Trans Biomed Eng* 1985;32:592-601
 32. Durand LG, Langlois YE, Lanthier T, et al. Spectral analysis and acoustic transmission of mitral and aortic valve closure sounds in dogs. Part 4: Effect of modulating cardiac inotropy. *Med Biol Eng Comput* 1990;28:439-445
 33. Durand LG, Langlois YE, Lanthier T, et al. Spectral analysis and acoustic transmission of mitral and aortic valve closure sounds in dogs. Part 2. Effects of neuromuscular blockade, sternotomy and pacemaker control, and a two-week recovery period. *Med Biol Eng Comput* 1990;28:278-286
 34. Durand LG, Langlois YE, Lanthier T, et al. Spectral analysis and acoustic transmission of mitral and aortic valve closure sounds in dogs. Part 1. Modelling the heart/thorax acoustic system. *Med Biol Eng Comput* 1990;28:269-277
 35. Billiar KL, Sacks MS. Biaxial mechanical properties of the natural and glutaraldehyde treated aortic valve cusp. Part I: Experimental results. *J Biomech Eng* 2000;122:23-30